A Cellular Potts Model simulating cell migration on and in matrix environments

MATHEMATICAL BIOSCIENCES
AND ENGINEERING
Volume **xx**, Number **0xx**, xx **20xx**

doi:10.3934/mbe.20xx.xx.xx

pp. **1–xx**

A CELLULAR POTTS MODEL SIMULATING CELL MIGRATION ON AND IN MATRIX ENVIRONMENTS

Marco Scianna

Department of Mathematics, Politecnico di Torino,
Corso Duca degli Abruzzi 24, 10129 Torino, Italy

Luigi Preziosi

Department of Mathematics, Politecnico di Torino,
Corso Duca degli Abruzzi 24, 10129 Torino, Italy

Katarina Wolf

Department of Cell Biology, Radboud University Nijmegen Medical Centre,
6500 HB Nijmegen, The Netherlands

(Communicated by the associate editor name)

Abstract. Cell migration on and through extracellular matrix is fundamental in a wide variety of physiological and pathological phenomena, and is exploited in scaffold-based tissue engineering. Migration is regulated by a number of extracellular matrix- or cell-derived biophysical parameters, such as matrix fiber orientation, pore size, and elasticity, or cell deformation, proteolysis, and adhesion. We here present an extended Cellular Potts Model (CPM) able to qualitatively and quantitatively describe cell migration efficiencies and phenotypes both on two-dimensional substrates and within three-dimensional matrices, close to experimental evidence. As distinct features of our approach, cells are modeled as compartmentalized discrete objects, differentiated in the nucleus and in the cytosolic region, while the extracellular matrix is composed of a fibrous mesh and of a homogeneous fluid. Our model provides a strong correlation of the directionality of migration with the topological extracellular matrix distribution and a biphasic dependence of migration on the matrix structure, density, adhesion, and stiffness, and, moreover, simulates that cell locomotion in highly constrained fibrillar obstacles requires the deformation of the cell's nucleus and/or the activity of cell-derived proteolysis. In conclusion, we here propose a mathematical modeling approach that serves to characterize cell migration as a biological phenomenon in healthy and diseased tissues and in engineering applications.

1. **Introduction.** Cell migration on and within tissues plays a critical role in a diverse array of processes, such as in developing embryos, where the coordinated movement of cells of different origin along extracellular matrix (ECM) layers is crucial for organogenesis, and migratory defects at all stages lead to severe embryonic malformations [42]. In adult organisms, cell movement is normally quiescent, except in immune surveillance or inflammation, where leukocytes actively migrate from blood vessels into infected tissues and then into the lymph node for effector

2000 *Mathematics Subject Classification.* Primary: 92B05, 92C15; Secondary: 92C42, 92C17.
Key words and phrases. cellular Potts model, extracellular matrix, cell migration.

.

functions [27], and in wound healing, where migration contributes to the repair of both basement membrane-underlaid epithelium and connective tissues. In pathologic conditions, cell migration is involved in chronic inflammatory diseases such as artheriosclerosis, or in cancer cell invasion into ECM and metastatization [69]. The process of cell migration is finally exploited in biomedical engineering applications for the regeneration of various tissues, such as cartilage, skin, or peripheral nerves *in vivo* or *in vitro* [11, 38, 75, 86].

Cell motile behavior is modulated by a spatiotemporally integrated set of multilevel mechanisms, that are influenced not only by the biochemistry of extracellular and intracellular signalling, but also by the biophysics of the surrounding environment, whose basic component is the Extracellular Matrix (ECM). The ECM forms in fact the architecture of a number of structures, i.e two-dimensional (2D) flat basement membranes, or three-dimensional (3D) connective tissues and can be described as a complex network of insoluble structural fibrous proteins such as collagen type I, and soluble glycosaminoglycans and glycoproteins, which, together, provide microstructural guidance cues and biochemical stimuli for moving individuals.

How does a cell migrate then on an in ECMs? For the basic program of cell migration over flat ECM substrates, four requirements have been identified: migrating cells (i) are morphologically polarized in the direction of motion, (ii) adhere dynamically to their environment via adhesive molecules, i.e. integrins, (iii) generate the force necessary for propulsion by contraction of cytoskeletal elements, and (iv) retract their rear ends [1, 45]. For migration within three-dimensional (3D) porous environments, in addition to these basic principles, the cell requires to steer its way throughout steric obstacles, [17, 66, 83]. This can be achieved by either (i) passage through constricted openings of the ECM by significant cell deformation and cytoskeletal force generation, or (ii) by activation of a cell-derived proteolytic machinery able to degrade matrix components and to open space for cell movement [23, 24, 41, 68, 84].

This basic motile behavior is further modulated by a number of mechanisms that include determinants from both the surrounding extracellular matrix and the cell itself (refer to [45, 83] and references therein) that we aim to systematically analyze by their combination with a modeling approach based on an extended Cellular Potts Model (CPM, [4, 33, 34, 36, 50, 71]). This is a grid-based Monte Carlo technique employing a stochastic energy minimization principle, used here to display the evolution of a cell population with distinct migratory behaviors that depend on matrix- or cell-derived parameters. As a distinct feature of our approach, each cell is modeled as a discrete compartmentalized object, differentiated into nucleus and cytosol, while the matrices are constituted of two components, an inhomogeneous fibrous collagen-like network, and a homogeneous interstitial medium.

The model is highly flexible, being able to characterize the migratory behavior of cells in several conditions, both on 2D substrata and in 3D ECMs. In the simulations, characteristics like cell shape and directionality are not imposed *a priori*, but are a result of the interaction with the matrix fibrous component. As an outcome, we focus on experimentally addressable characteristics of cell locomotion, i.e., cell overall displacement, velocity and persistence time, and cell shape, predicting how these quantities are influenced by manipulations of properties of either the matrix (i.e., adhesive ligands, fiber distribution, pore size, elastic modulus), or the cell (i.e., adhesive strength, deformability, and proteolysis).

Consistent with experimental observations, our findings provide evidence for a biphasic cell migratory behavior for planar substrate in response to variations of the number of matrix ligands or adhesion strength, with maximal movements at intermediate values. In 3D matrix environments, the geometrical distribution of the collagenous network, such as matrix alignment or pore size, or the matrix elasticity will be demonstrated to affect cell behavior in a similar way. Further, the cell compartmentalization allow to discern the mechanical rigidity of the nucleus that, being higher than the cytosol, limits the migration capacity of the entire cell. Finally, we will include ECM-directed proteolysis, resulting in enhanced migration in restricted environments.

The remaining parts of this publication are organized as follows: in Section 2 (Mathematical Model), we clarify the assumptions on which our approach is based. The computational findings are then presented in Section 3 (Results), where we separately analyze both topological and mechanical features of different matrices, and variations in cell biophysical properties on the cell migratory behavior. Finally, the results are discussed in Section 4 (Discussion), and in Section 5 (Appendix), we provide details on the estimates of statistical quantities used to characterize the migratory capacity of moving individuals.

2. **Mathematical Model.**

The above introduced cell-ECM system is modeled at the mesoscopic level using an extended Cellular Potts Model, a grid-based stochastic approach, which describes the behavior of single individuals and their interactions with the local microenvironment in energetic terms and constraints. The simulation domains are d-dimensional regular lattices (i.e., numerical repeated graphs formed by equivalent sites) $\Omega \subset \mathbb{R}^d$, where $d = 2, 3$ (we will specify the spatial dimensions according to the specific application described in the following). Each d-dimensional site $\mathbf{x} \in \Omega \subset \mathbb{R}^d$ is labeled by an integer number, $\sigma(\mathbf{x})$, which can be interpreted as a degenerate *spin* originally coming from statistical physics [40, 61]. As classically adopted in CPM applications, a neighbor of $\mathbf{x}$ is identified by $\mathbf{x}'$, while its overall neighborhood by $\Omega_{\mathbf{x}}^{'}$, i.e. $\Omega_{\mathbf{x}}^{'} = \{\mathbf{x}' \in \Omega : \mathbf{x}' \text{ is a neighbor of } \mathbf{x}\}$. Subdomains of contiguous sites with identical spin form discrete objects Σ_σ (i.e., $\Sigma_{\overline{\sigma}} = \{\mathbf{x} \in \Omega : \sigma(\mathbf{x}) = \overline{\sigma}\}$), which are characterized by an object type, $\tau(\Sigma_\sigma)$.

The spatial domain is then occupied by cells, ECM fibers and physiological liquid. The simulated cells, η, are defined as compartmentalized units, composed of two subregions which, in turn, are classical CPM objects Σ_σ: the nucleus, a central cluster of type $\tau = N$, and the surrounding cytosol, of type $\tau = C$. Each cell compartment is obviously characterized, as an additional attribute, by the cluster id $\eta(\Sigma_\sigma)$ to identify the individual it belongs to. The cell population resides either on a two-dimensional (2D) or within a three-dimensional (3D) ECM.

The environments surrounding the cells is differentiated into a homogeneous medium-like state, $\tau = M$, and an inhomogeneous collagen-like state, $\tau = F$. The medium-like state reproduces the mixture of soluble components (among others, proteoglycans and glycoproteins in water), which compose the interstitial fluid constant in viscosity. It is assumed to be isotropically distributed throughout the simulation domain, forming no large-scale structures. The collagen state represents instead a network of insoluble macromolecules, such as collagen, that associates into first-order fibrils and second-order fibers and displays the most abundant structure in mammalian tissues. Each fibrous component is treated as CPM standard and non-compartmentalized CPM objects Σ_σ. Dimensions, density and distribution of

the fibrous structures will be specified in next sections and will reproduce 2D and 3D matrix types, respectively, typically employed for *in vitro* assays. The inclusion of an explicit two-component matrix environment, already present in some other CPM applications [5, 32, 49, 67], is a fundamental aspect of this work: it allows an accurate analysis of how cells migratory behavior is influenced by the heterogeneous fibrillar extracellular environment and therefore by the ECMs specific biophysical and biomechanical properties while they glide in medium of constant and homogeneous physical properties.

The simulated cell culture evolves to iteratively and stochastically reduce the free energy of the overall system, defined by the so-called *hamiltonian* H, whose expression will be clarified below. The core algorithm is a modified Metropolis method for Monte Carlo-Boltzmann dynamics [36, 52], which is able to implement the natural exploratory behavior of biological individuals. Procedurally, at each time step t in the model, called Monte Carlo Step (MCS), a lattice site, $\mathbf{x}_{source}$, is selected at random and assigns its spin, $\sigma(\mathbf{x}_{source})$, to one of its unlike neighbors, $\mathbf{x}_{target} \in \Omega'_{\mathbf{x}} : \mathbf{x}_{target} \notin \Sigma_\sigma$, also randomly selected. The net energy difference due to the proposed change of domain configuration, $\Delta H|_{\sigma(\mathbf{x}_{source})\rightarrow\sigma(\mathbf{x}_{target})} = H_{(after\ spin\ copy)} - H_{(before\ spin\ copy)}$, is then evaluated. The trial lattice update is finally accepted with a Boltzmann-like probability function:

$$\begin{aligned} &P(\sigma(\mathbf{x}_{source}) \rightarrow \sigma(\mathbf{x}_{target}))(t) = \\ &= \tanh(\varepsilon T_{\Sigma_{\sigma(\mathbf{x}_{source})}}(t)) \min\{1, e^{-\Delta H|_{\sigma(\mathbf{x}_{source})\rightarrow\sigma(\mathbf{x}_{target})}/T_{\Sigma_{\sigma(\mathbf{x}_{source})}}(t)}\} \end{aligned} \tag{1}$$

where $T_{\Sigma_{\sigma(\mathbf{x}_{source})}}(t) \in \mathbb{R}^+$ is a Boltzmann temperature. It does not reflect any conventional thermal temperature but it is a measure of the *mobility* of the moving compartment $\Sigma_{\sigma(\mathbf{x}_{source})}$. The specific form of (1) is a definitive improvement of the classical function used in all CPM applications (formally recovered in the limit $\varepsilon \rightarrow \infty$). The standard transition probability has in fact a significant weakness in the fact that, in the case of non positive net energy differences caused by the proposed displacement ($\Delta H|_{\sigma(\mathbf{x}_{source})\rightarrow\sigma(\mathbf{x}_{target})} \leq 0$), each element $\Sigma_{\sigma(\mathbf{x}_{source})}$ is certainly going to move, regardless of its intrinsic motility, given by $T_{\Sigma_{\sigma(\mathbf{x}_{source})}}$, which lacks biological realism. For example, a "frozen" cell (i.e., with negligible intrinsic motility) does not extend its pseudopods towards a chemical source even if it senses a high chemotactic gradient (which, in the absence of other external forces, would result in $\Delta H \ll 0$). This issue is addressed using transition probabilities similar to (1), i.e. which take into account the object motility $T_{\Sigma_{\sigma(\mathbf{x}_{source})}}$ also in the case of energetically favorable displacement attempts. Indeed, the choice of function tanh is a modeling option: more in general, the reader can use any other continuous and increasing law $p(T_{\Sigma_{\sigma(\mathbf{x}_{source})}}(t)) : \mathbb{R}^+ \mapsto [0, 1]$ characterized by

$$\begin{cases} p(0) = 0; \\ \\ \lim\limits_{T_{\Sigma_{\sigma(\mathbf{x}_{source})}} \rightarrow +\infty} p(T_{\Sigma_{\sigma(\mathbf{x}_{source})}}) = 1, \end{cases} \tag{2}$$

as detailly commented in [71]. In particular, for $\tau(\Sigma_{\sigma(\mathbf{x}_{source})}) = N$, $T_{\Sigma_{\sigma(\mathbf{x}_{source})}} = T_N$ gives a measure of the relative motility of the cell nucleus, while, for $\tau(\Sigma_{\sigma(\mathbf{x}_{source})}) = C$, $T_{\Sigma_{\sigma(\mathbf{x}_{source})}} = T_C$ is a measure of the intrinsic motility of the overall individual, as it gives the frequency of the ruffles of its cytosol (which, on a molecular level, are determined by polarization/depolarization processes of the actin cytoskeleton, refer to [53, 60, 64] and references therein). Finally, for $\tau(\Sigma_{\sigma(\mathbf{x}_{source})}) = F$, $T_{\Sigma_{\sigma(\mathbf{x}_{source})}} = T_F$

determines the vibration degree of matrix fibers. For each cell, T_N is a low value (< 1), resulting in a more passive motion of the nucleus (with respect to the cell membrane), which, unable to have an autonomous movement, is dragged by the surrounding cytosol, characterized instead by a high $T_C \gg 1$ (see our recent work [70] for a detailed mechanical explanation). In most simulations, the matrix fibers are instead assumed to be fixed by setting $T_F = 0$.

For any given time t, the system *hamiltonian*, whose minimization drives the evolution of the system, is defined as:

$$H(t) = H_{shape}(t) + H_{adhesion}(t). \tag{3}$$

H_{shape} models the geometrical attributes of simulated objects (both subcellular compartments and matrix threads), which are written as non-dimensional relative deformations in the following quadratic form:

$$\begin{aligned} &H_{shape}(t) = H_{volume}(t) + H_{surface}(t) = \\ &= \sum_{\Sigma_\sigma} \left[\kappa_{\Sigma_\sigma}(t) \left(\frac{v_{\Sigma_\sigma}(t) - V_{\tau(\Sigma_\sigma)}}{v_{\Sigma_\sigma}(t)} \right)^2 + \nu_{\Sigma_\sigma}(t) \left(\frac{s_{\Sigma_\sigma}(t) - S_{\tau(\Sigma_\sigma)}}{s_{\Sigma_\sigma}(t)} \right)^2 \right], \end{aligned} \tag{4}$$

depending on the actual volume and surface of the object, $v_{\Sigma_\sigma}(t)$ and $s_{\Sigma_\sigma}(t)$ (which reduce, respectively, to its surface and perimeter in two dimensions), as well as on the same quantities in the relaxed state, $V_{\tau(\Sigma_\sigma)}$ and $S_{\tau(\Sigma_\sigma)}$, corresponding to its initial measures. The formulation of (4) allows to have finite energetic contributions, as well as a blow up in the case of $v_{\Sigma_\sigma}(t), s_{\Sigma_\sigma}(t) \to 0$, see again [71] for a detailed explanation. $\kappa_{\Sigma_\sigma}(t)$ and $\nu_{\Sigma_\sigma}(t) \in \mathbb{R}^+$ are mechanical moduli in units of energy: in particular, $\kappa_{\Sigma_\sigma}(t)$ refer to volume changes, while $\nu_{\Sigma_\sigma}(t)$ relates to the degree of deformability/elasticity of the related object, i.e. the ease with which it is able to remodel. Indeed, assuming that cells do not significantly grow during migration, the fluctuations of their volumes are kept negligible with high constant values $\kappa_{\Sigma_\sigma} = \kappa \gg 1$, for any individual η and for Σ_σ such that $\tau(\Sigma_\sigma) = \{N, C\}$. Moreover, cells moving in matrix environments are typically deformable, but their nuclei show a higher rigidity w.r.t. the cytoplasm region: therefore, for any η and for Σ_σ such that $\tau(\Sigma_\sigma) = C$, we set $\nu_{\Sigma_\sigma} = \nu_C \ll 1$, while and for Σ_σ such that $\tau(\Sigma_\sigma) = N$, we set $\nu_{\Sigma_\sigma} = \nu_N \gg 1$. The extracellular environment is instead assumed to have homogeneous mechanical and microstructural properties: in particular the matrix fibers are assumed to be rigid by setting $\kappa_F = \nu_F \gg 1$. However, it is useful to underline that in the following we will analyze how the explicit variation of fiber and nucleus stiffness will affect cell migratory phenotypes within three-dimensional matrices.

$H_{adhesion}$ is the general extension of Steinberg's Differential Adhesion Hypothesis (DAH) [36, 76, 77]. In particular, it is differentiated into the contributions of either the generalized contact tension between the nucleus and the cytoplasm within the same cell, or the effective adhesion between a cell and both the medium and the fibrillar matrix component, and, in case of collision, between cells:

$$\begin{aligned} &H_{adhesion}(t) = H^{int}_{adhesion}(t) + H^{ext}_{adhesion}(t) = \\ &= \sum_{\substack{\mathbf{x}\in\Omega, \mathbf{x}'\in\Omega'_{\mathbf{x}} \\ \eta(\Sigma_{\sigma(\mathbf{x})}) = \eta(\Sigma_{\sigma(\mathbf{x}')}) \\ \Sigma_{\sigma(\mathbf{x})} \neq \Sigma_{\sigma(\mathbf{x})}}} J^{int}_{\tau(\Sigma_{\sigma(\mathbf{x})}), \tau(\Sigma_{\sigma(\mathbf{x}')})} + \sum_{\substack{\mathbf{x}\in\Omega, \mathbf{x}'\in\Omega'_{\mathbf{x}} \\ \eta(\Sigma_{\sigma(\mathbf{x})}) \neq \eta(\Sigma_{\sigma(\mathbf{x}')}) \\ \Sigma_{\sigma(\mathbf{x})} \neq \Sigma_{\sigma(\mathbf{x}')}}} J^{ext}_{\tau(\Sigma_{\sigma(\mathbf{x})}), \tau(\Sigma_{\sigma(\mathbf{x}')})}. \end{aligned} \tag{5}$$

The Js are binding energies per unit area, which are obviously symmetric. In particular, $J^{int}_{N,C}$ implicitly models the forces exerted by intermediate and actin filaments, and microtubules to anchor the nucleus to the cell cytoskeleton and preventing cells from fragmenting, while $J^{ext}_{C,C}$ represents the local adhesive strength between neighboring cells, a measure of the local quantity of active and exposed cadherin molecules. $J^{ext}_{C,M}$ and $J^{ext}_{C,F}$ evaluate instead the heterophilic contact interactions between cells and matrix components. Specifically, $J^{ext}_{C,M}$ and $J^{ext}_{C,F}$ are a measure of the affinity between cell surface adhesion complexes (i.e. sugar-binding receptors or integrins) to either non-solid (i.e. glycosaminoglycans in medium) or solid (i.e. fibrillar collagen) extracellular ligands, respectively [73]. In particular, given $J^{int}_{N,C} \ll 0$ to prevent cell splitting, we assume $J^{ext}_{C,F} < J^{ext}_{C,M}$ since, as widely demonstrated in literature, most cell lines in standard conditions adhere more strongly with the fibrous part of the extracellular matrix rather than with its soluble component (see [78] and references therein). $J^{ext}_{C,C}$ is instead kept high to avoid cell-cell adhesive interactions upon accidental cell collisions that may affect the cell's movement. Setting constant and homogeneous values for the bond energies Js corresponds to assuming a uniform distribution of adhesion molecules on cell surfaces and of ligands in the external environment, without any change during the observation time. A summary of values of all the model parameters used in the simulations is given in Table 1.

Finally, it is useful to underline that, while in the 2D case cells can freely move on the entire extracellular ECM-coated surface, in 3D environments, the collagenous part of the matrix represents instead a potential steric obstacle for moving individuals that they must overcome during motion, whereas, in parallel, within interstitial medium they can freely float.

3. **Results.**

3.1. **Simulation Characteristics.**

To apply the Cellular Potts Model to simulate and describe cell migration on and in ECM matrices, we start with default cell-ECM conditions and subsequently adapt them to specific conditions, such as matrix orientation, density, adhesiveness etc., relevant for migration *in vitro* and *in vivo*.

The basic CPM in both 2D and 3D conditions contains certain common spatial and temporal characteristics. The spatial simulation domain Ω is a regular d-dimensional lattice with periodic boundary conditions and a basic grid size of 1.3 μm. In all the bidimensional simulations, $\Omega \subset \mathbb{R}^2$ represents a 3.5 cm (i.e., $2.69 \cdot 10^4$-site-width) side-length squared section of an experimental dish, which is commonly used for planar migration assays [16]. In the three-dimensional case, $\Omega \subset \mathbb{R}^3$ reproduces instead an experimental scaffold with a volumetric extension of 1 cm^3 (formed by $4.55 \cdot 10^{11}$ cubic voxels). The temporal resolution of the model is the MCS which is set to correspond to 2 s to compare cellular dynamics with experimental observations. All the performed simulations last 12 h ($\approx$ 21600 MCS) to ensure the development of sufficient long migration paths. The choice of this observation time allows also to not consider critical events, such as cell apoptosis and duplication, which would significantly affect cell migratory behavior (i.e., during the mitotic process, cells are prohibited to migrate [1]).

The basic cell-matrix model to be simulated consists of a heterogeneous ECM of fibrillar and amorph ('medium') components hosting a cell population of low density to allow for isolated motions with very rare cell encounters.

TABLE 1. Model Parameters

Parameter	Description	Value	Reference
V_N	surface of cell nucleus in 2D	34.7 [μm^2]	[1]
S_N	perimeter of cell nucleus in 2D	20.8 [μm]	[1]
V_C	surface of cell cytosol in 2D	104.3 [μm^2]	[1]
S_C	perimeter of cell cytosol in 2D	62.6 [μm]	[1]
V_N	volume of cell nucleus in 3D	155.2 [μm^3]	[1]
S_N	surface of cell nucleus in 3D	138.8 [μm^2]	[1]
V_C	volume of cell cytosol in 3D	1076.3 [μm^3]	[1]
S_C	surface of cell cytosol in 3D	694.6 [μm^2]	[1]
V_F	surface of matrix fibers	20 [μm^2]	[8, 63, 65]
S_F	length of matrix fibers	20 [μm]	[8, 63, 65]
ε	coefficient of Boltzmann probability	1	
T_N	motility of cell nucleus	0.5	[70]
T_C	motility of cell cytosol	9	[70]
T_F	motility of matrix fibers	0	
κ	compressibility of cell volume	10	
ν_N	rigidity of cell nucleus	8.5	[26, 70]
ν_C	rigidity of cell cytoplasm	0.8	[26, 70]
ν_F	rigidity of matrix fibers	11	
κ_F	compressibility of matrix fibers	11	
$J^{int}_{N,C}$	generalized intercellular adhesion	-20	[71]
$J^{ext}_{C,C}$	cell-cell adhesive strength	12	
$J^{ext}_{C,M}$	cell-medium adhesive strength	6.5	[78]
$J^{ext}_{C,F}$	cell-fiber adhesive strength	4.5	[78]
D_m	diffusion constant of MMPs	5^{-4} [μm^{2}s^{-1}]	[68, 81]
λ_m	on-rate constant of MMP decay	$2 \cdot 10^{-3}$ [s^{-1}]	[81]
π_m	on-rate constant of MMP production	$5 \cdot 10^{-3}$ [s^{-1}]	[81]

In all 2D simulations, we plate $1 \cdot 10^3$ cells/cm^2, as done in [16], while in all 3D simulations, we embed $2 \cdot 10^3$ cells/cm^3, reproducing the cellular density of the experimental migration assays performed in [37]. The cells that interact with collagen-like fibers, i.e. fibroblasts or cancer cells of epithelial or mesenchymal origin, display initially a round non-migratory unpolarized morphology: therefore, as default conditions, we start with round flat disks with a central round nucleus in 2D, and as spheres with a spherical nuclear compartment in 3D. In both cases, their overall diameter is 10 grid sites ($\approx$ 14 μm), while the nucleus is 5 grid sites ($\approx$ 7 μm) in diameter. For the reader's convenience, we underline that the entire volume (resp, the area in 2D) of a cell is the sum of the volume (resp, the area in 2D) of the nucleus and of the cytosolic region, while its external surface (resp, the perimeter in 2D) is instead the difference between the surface (resp, the perimeter) of the cytosol and the surface (resp, the perimeter) of the nucleus. These dimensions, given in Table 1, reflect the mean measures of typical eukariotic cells except white blood cells [1].

In our model, we set the length of a collagen-like fiber equal to 15 lattice sites ($\approx$ 20 μm). Its thickness would generally range between 100 nm and 0.5 μm [8, 63, 65],

and therefore it would be substantially smaller than the grid resolution. However, following a common approach for CPM applications [32, 67], we here accorded a fiber the measure of a single site, so that it is reproducible in the domain Ω. Each simulated fiber therefore is assumed to contain nearly 10^6 collagen-like molecules, given that a single matrix protein is approximately 300-600 nm long and 1.5-5 nm wide [1]. Finally, for sake of simplicity, we will use the term fiber for both the basic short ECM structure ($\approx$ 20 μm long threads) simulated for the 2D condition, and the long structure crossing the entire spatial domain of the 3D cubic network.

3.2. **Isotropic 2D and 3D Matrices.** We first test the model for standard matrices containing an isotropic, moderately dense, fibrous network in both two and three dimensions. As planar substrate, we distribute $3 \cdot 10^5$ flat collagen-like fibers in each x and y-direction of the 3.5 cm-side length dish, yielding a density of 500 fibers/mm^2, see left top panel of Fig. 1(A). The analogous isotropic 3D scaffold consists of a regular cubic mesh of collagen fibers creating a uniform pore distribution of 10 μm width (i.e., the same order of magnitude of the initial cell diameter, see Fig. 1(A), right top panel). We simulate a regular fibrous network to avoid the minor heterogeneities often experienced in experimental matrices, where the distribution of the threads and the relative pore diameters is only roughly constant [47, 54, 82]. As shown in the wind-rose graph (Fig. 1(B)), when cells migrate on both 2D and in 3D matrices, the selected cell paths display a random walk, without preferred direction, in the absence of biasing chemical gradients or matrix anisotropies.

Such migratory path structures and quantitative parameters are consistent with experimental results for both 2D and 3D porous ECMs, such as for human adult vascular smooth muscle cells (HSMCs) plated on flat type IV collagen (CnIV) substrates of similar concentrations [16] or human glioma cells plated on polyacrylamide ECMs [79], and for different fibroblastic and cancerous cell lines migrating within 3D fibrous matrices of similar geometrical and structural properties, i.e., NR6 mouse fibroblasts in collagen-glycosaminoglycan matrices [37], or human melanoma cells in collagen lattices [25]. Indeed, these comparisons provide confidence in the choice of parameters describing the biophysical and mechanical properties of the simulated cell-ECM system.

3.3. **Anisotropic 2D and 3D Matrices.** Next, we analyze the migratory characteristics of a cell population in the case of anisotropic matrices. In particular, we keep fixed the quantity of fibers as displayed in Fig. 1, but progressively change their distribution by increasing their number along the same x-direction, leaving remaining fibers disposed in their standard direction (Fig. 2(A, B; top rows)). The alignment of the matrix is quantified by evaluating a proper index, that can be called *aligned index*, given by

$$N_{align} = \frac{(d\, n_x/n_{tot}) - 1}{d - 1}, \tag{6}$$

where d is the dimension of the domain, n_x the number of threads along the x-direction and n_{tot} their overall number. This quantity scales the percentage of fibers aligned along the x-direction, so that it is zero in the case of isotropic networks and 1 in the case of fully aligned matrices.

As a result, for both 2D and 3D migration, the paths gradually adapt towards anisotropic random walks, in particular, the directional cell motion increases towards the principal direction of alignment, see Fig. 2(A,B; bottom rows). Interestingly, the cells final average velocity and MSD remain constant despite increasing

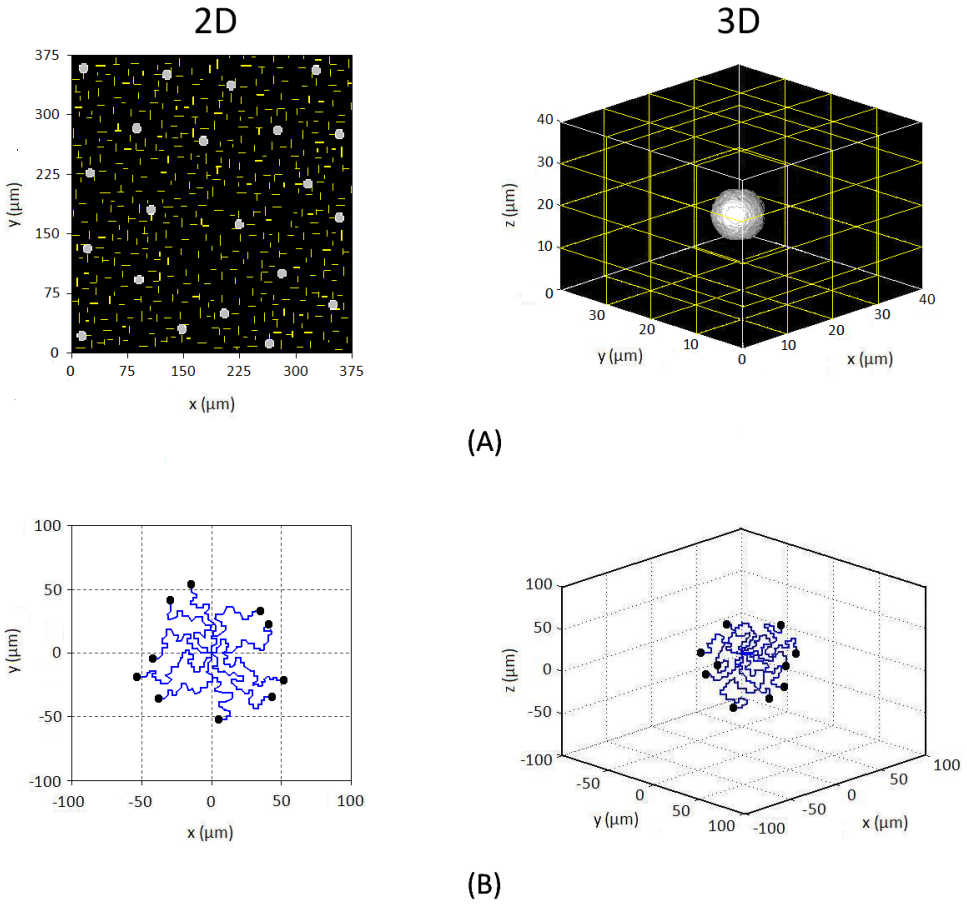

FIGURE 1. Standard cell-ECM models and migration in two and three dimensions. Top panels (A): sections of the simulation domain Ω of both the 2D and the 3D case. Depicted are standard two-component substrates containing both an isotropic fibrous ECM of moderate density (yellow stripes) and the medium (black), and cells. In the 2D model, 500 fibers/mm^2 fibers are distributed equally and in both $x-$, $y-$directions. In the 3D scaffold, matrix fibers are assembled into a regular cubic mesh, with a uniform distribution of pores of 10 μm side length. As an initial condition, a sparse population of cells is plated on or into the matrices. Bottom panels (B): cell migration on or within the above-represented isotropic ECMs. Wind-rose graphs showing 10 randomly chosen cell tracks over 12 h. Black circles represent the ending location of each cell center of mass. In both conditions, cells display a Brownian random movement with net final displacement ca. 50 μm, MSD ca. $9 \cdot 10^4 \pm 0.5 \cdot 10^3$ μm^2 (median $8.8 \cdot 10^4$ μm^2), and velocity ca. 10 ± 0.6 μm/h (median 9.7 μm/h). As reproduced from selected cell paths, the persistence time is low (ca. 1.5 ± 0.2 h, median 1.2 h). Here and in the following all values are given as means $\pm$ s.d. over 50 randomly chosen individuals (see appendix). The cell migratory behavior is consistent with the extracellular environment isotropy, and the absence of chemical gradients or other directional biases.

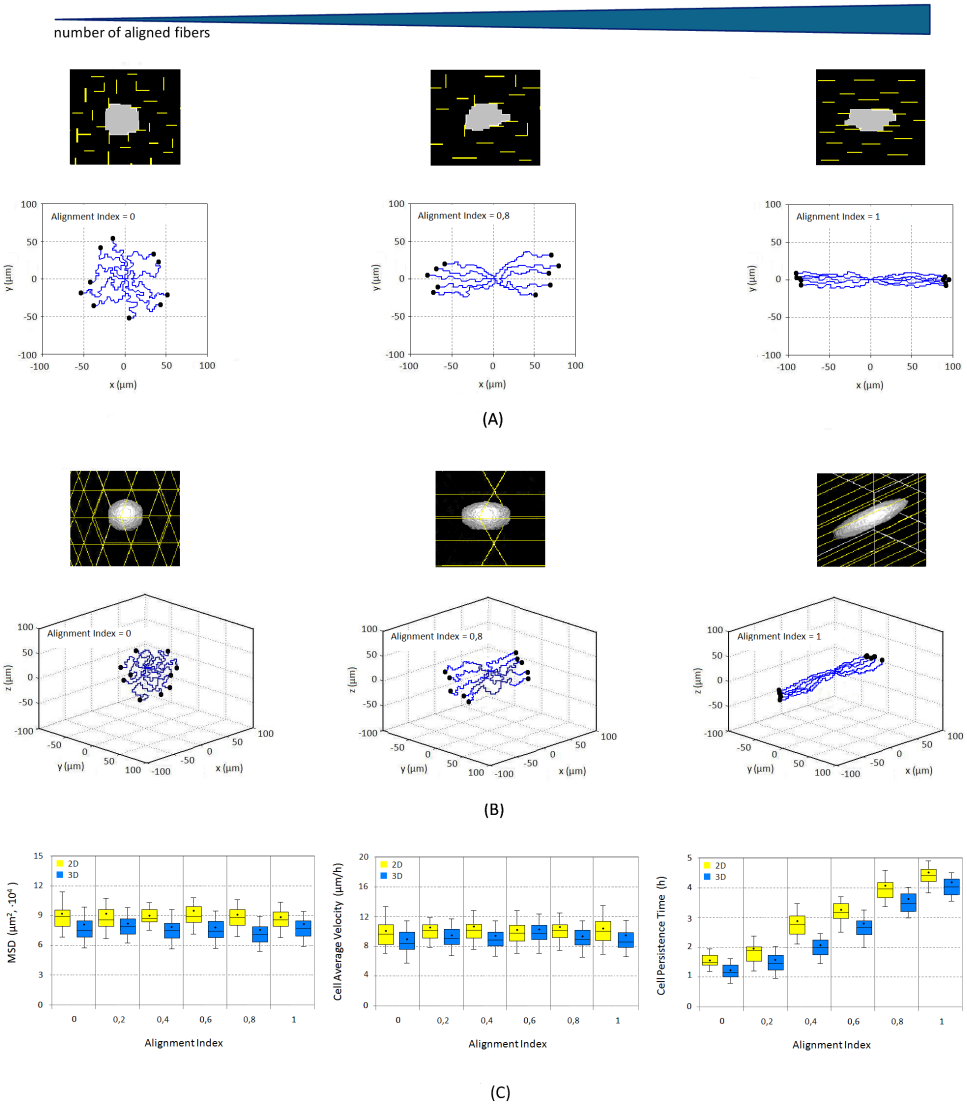

FIGURE 2. Orientation of cell migration along matrix fiber topology. Both on 2D (A) and within 3D matrix (B), the overall number of basic fibers remains fixed with respect to the standard simulations of Fig. 1, while their percentage along the x-axis is increased. The alignment of the matrices is quantified by the alignment index N_{align}, defined in (6), which is 0 in the case of isotropic networks and 1 for fully aligned ECMs. (A, B; top rows) Three specific cases for simulation-obtained threads (yellow) and cell morphologies. (A, B; bottom rows) Wind-rose graphs show 10 randomly chosen cell tracks over 12 h. (C) Cell mean square displacement (MSD), average velocity and persistence time for both 2D and 3D matrix, displayed with box-and-whisker plots, with box edges as 25^{th} and 75^{th} percentiles and whiskers as 10^{th} and 90^{th} percentiles. Horizontal lines, median; large black dots, mean of the distribution. Statistical significance ($p < 0.05$) was determined for motile fraction data by the Students' t-test and for non-normally distributed data sets by the Kolmogorov-Smirnov test over 50 randomly chosen individuals (see also appendix). The directional component of cell motion increases as all fibers align, with no change in cell speed.

substrate orientation, with very similar values for both 2D and 3D conditions. However, the cell's 2D and 3D directed motile behavior in response to fiber distribution directly correlate with a strong increase in time (up to 5 hours) that cells are able to perform persistent (no back-and-forth) movement. Therefore, ECM geometry and architecture directly impact on the migration pattern of individual cells. The directionality of cell movement is here not introduced *a priori*, but is a direct result of well-defined *directional-guidance cues* provided by the specific matrices. The anisotropy of the matrices induces in fact a re-orientation of moving cells in the direction of the threads (i.e., with the formation of clearly distinguishable leading and trailing edges, see Fig. 2(A, B; top rows)) and the consequent motion along them, which is no longer an isotropic Brownian movement, but a highly biased locomotion.

The efficiency of cell migration is highly affected by the orientation and spacing of matrix components and its adhesive ligands, resp., as experimentally proven by lithographic and microprinting techniques creating 1D ECM pathways that offer geometric guidance and adhesive structures at a microscale [9, 17, 19, 46]. Moreover, several experimental models have demonstrated the cell's preference to migrate along aligned matrix fibers within 3D environments, such as fibroblasts in collagen [15] or neuronal cells in fibrin substrates [18]. Lastly, *in vivo* intravital imaging studies of carcinoma cells in the mammary fat pad have pointed out the preferential chemotactic movement of invasive malignant cells along thick bundles of collagen fibers offering a 2D surface towards blood vessels [13], while in the lymph node paracortex, the aligned microarchitecture of collagen and fibronectin fibers ensheathed by fibroblastic reticular cells significantly influenced the migratory behavior of T-cells [3].

3.4. **Pore Size in 3D Matrices.** The ECM fibers and bundles in *in vivo* tissues that provide directional guidance cues are arranged into structures that create pores and gaps of strongly varying local densities [82]. Connective tissues, i.e. of the skin, are categorized into loose and dense extracellular tissues, and pores size are formed irregularly and form gaps between ca. 1 to 1000 μm [82]. As another example, in progressing tumors the surrounding tumor stroma changes into fibrous tissue over time that, concomitantly, may change its structural architecture [14]. These matrices of different densities provide physical barriers to different extents together with varying gap sizes for moving cells.

In the CPM model, we simulate the effect of varying substrate fiber density on cell migration in 3D networks, where matrix fiber form a regular cubic mesh, with uniform pore sizes that decrease due to increment in the number of fibers. In result, the simulations predict a bimodal behavior of cell velocity and persistence (Fig. 3(A)). At low numbers of bundles the 3D scaffold constitutes a sparse network, resulting in pores significantly larger than the diameter of the characteristic cell shape. In this case cells exhibit a short-range movement while their body remains in a stationary ameboid-like state, regardless of their deformation ability, presumably because the distance from the nearest matrix fiber is too high to experience adhesive interactions that enable them to extend their membrane (Fig. 3(B)). On the other hand, the formation of pore diameters of cellular or slightly subcellular ranges allows cells to physically interact with fibers in all three spatial directions and is associated with most efficient migration rates [25]. In this case, migrating cells apply an elongated morphology and slightly reduce their diameters to ca. 8-10

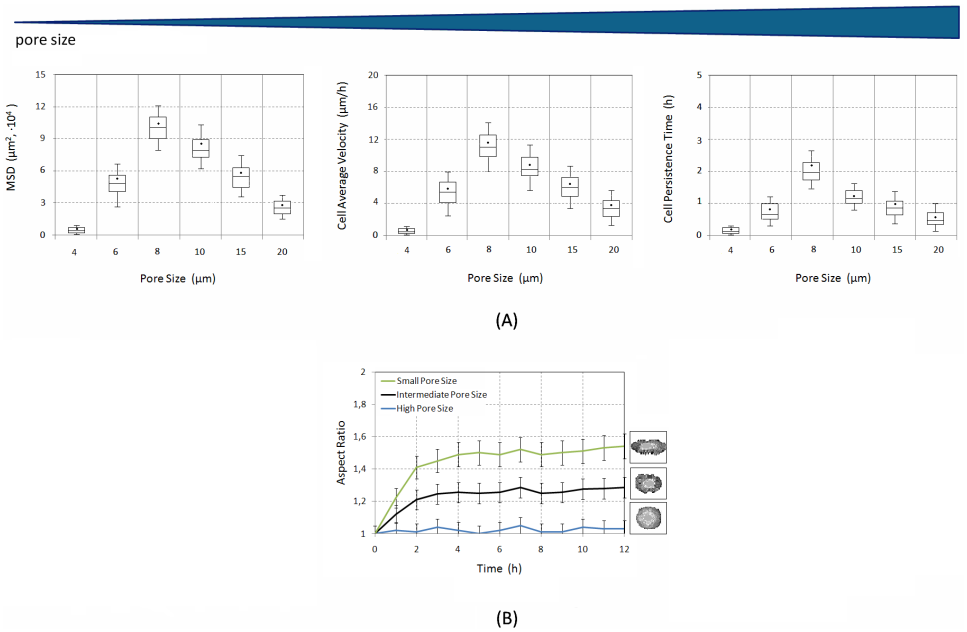

FIGURE 3. Dependency of cell migration and morphology on the pore size in 3D matrices. Originating from the isotropic scaffold in Fig. 1, an increasing number of collagen fibers is introduced, which leads to a decrement in pore sizes. (A) Box-and-whisker plots (means, lines; medians, dots; see appendix) display cell MSD, cell average velocity, and persistence time from 50 randomly selected cells migrating within matrices of decreasing pore size. (B) Cell morphological transitions (evaluated by the cell aspect ratio, see appendix) over time upon varying pore dimensions of 20 μm blue line, 10 μm black line, and 5 μm green line. Cell morphologies are obtained from the simulations. Cell elongation increases with decrements of pore size (i.e., increments in fiber number) until a threshold value, defined by the measure of the cell region containing the nucleus, that can not deform further. As in the following, each value in the plot is shown as mean $\pm$ s.d. over 50 randomly chosen individuals (see also appendix).

μm. Finally, an increase in the abundance of 3D matrix threads results in the formation of a scaffold characterized by small pores with limited available space (i.e., half of a cell diameter or less), and a substantially decreased cell migration rate is predicted. Even long cytosol formations (Fig. 3(C)) are in fact not sufficient to pass through such steric hindrances, as the nucleus can not significantly deform (ν_N is high), causing the overall individual to be confined in a small area. In a following section, the migration ability of cells depending on their nuclear deformability will be examined. In summary, cells display a biphasic relationship that reveals most optimal migration at pore sizes at cellular or somewhat subcellular diameters, and diminishes at gaps greatly bigger or smaller than the moving cell diameter.

The outcomes of our models are consistent with the relative observations provided in the experimental literature. In 3D environments, neutrophil migration (both velocity and directional coefficient) has been reported to vary in a biphasic manner with the gel pore size [41], while mouse fibroblasts have been observed to

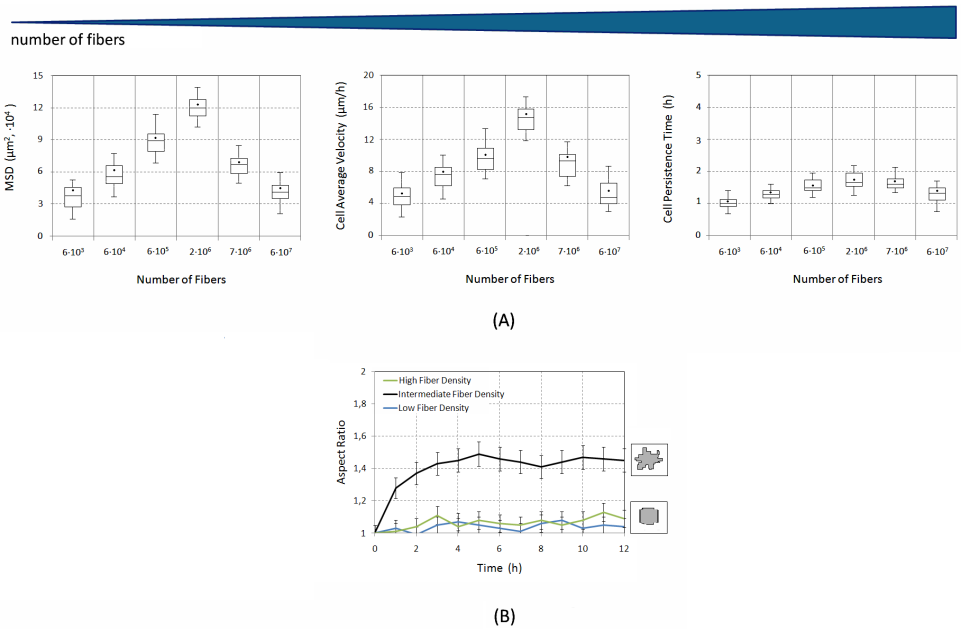

FIGURE 4. Biphasic relationship of cell motility and related morphology with fiber number on 2D substrates. The number of fibers is stepwise increased from $6 \cdot 10^3$ to $6 \cdot 10^7$ per dish (with $6 \cdot 10^5$ fibers per dish representing the standard case). All other parameters remain unchanged, such as in the standard case of Fig. 1. (A) The box-and-whisker plots (means are lines, medians are dots, see appendix) represent cell MSD, average velocity, and persistence time from 50 randomly selected cells. (B) Changes in aspect ratio during migration over 12 hours upon varying fiber density. Number of fibers are: $6 \cdot 10^3$ (blue, low density), $2 \cdot 10^6$ (black, intermediate density), and $6 \cdot 10^7$ (green, high fiber density). Migration-associated lamellipodial ruffling is maximal at intermediate fiber densities, whereas at low and high number of threads cells remained roundish, associated with little migration.

migrate more significantly in collagen-glycosaminoglycan (CG) scaffolds featuring pore sizes somewhat smaller than cellular dimensions, whereas they have exhibited less dispersion in matrices with larger pores [37].

3.5. **Cell-Fiber Adhesiveness.** Cell-matrix adhesion is mainly mediated by integrins on the cell surface that form a linker to connect ECM to the cytoskeleton and signaling pathways. Adhesion can be modulated by a number of parameters, such as (i) the number of substratum ligands, (ii) the expression and activation levels of integrins, and (iii) the resulting integrin-ligand binding affinity, which can be reduced by $\beta 1$ integrin antibodies that block integrin binding epitopes to ECM or by soluble ligands that compete with ligand binding, or can be enhanced by integrin activating agents.

From the mathematical point of view, adhesiveness is modeled by both fiber density of the substrate or the cell-fiber adhesion parameter $J^{ext}_{C,F}$.

3.5.1. *Substrate Density of 2D Matrices.* As mentioned above, adhesion depends on the number of substratum ligands applied here as varying fibril densities on 2D surfaces. Such an application will induce a change in adhesive properties without steric consequences thereby representing a controlled approach. In contrast, since the modeling of varying fiber numbers in a 3D porous lattice will concomitantly change available space and thereby interdependent pro-migratory co-parameters, we excluded this approach from analysis.

We simulate here migration over a surface containing an increasing amount of matrix fibers distributed equally and isotropically along the $x-$ and $y-$directions. Cell spreading, characterized by an increase of cell surface area over time [12] remains nearly fixed (i.e., by high values of κ). Therefore, the resulting simulations cannot capture the variation of cell contact area with the underlying substrate, characterizing cell spreading in 2D assays. However, the migratory structure of the cells, characterized for instance by the elongation of pseudopods, is clearly quantified by the aspect ratio, defined in the Appendix.

Indeed, migration efficiencies develop a bell-shaped distribution from low towards high fiber numbers with a maximum at intermediate fiber numbers (Fig. 4(A)). At low ligand density, cells are unable to find sufficient collagen-like sites to attach and, in consequence, do not significantly displace. At the other extremum, an abundance of substratum ligands will lead to the formation of stable focal adhesions and, hence, low detachment and migration rates. Concomitantly, in both cases, cell remains in ameboid-like shapes (see Fig 4(B), lower inset).

At intermediate fiber densities, relatively short-lived focal adhesions will form resulting in optimization of attachment-detachment cycles and in maximal cell movement. The optimization of focal adhesion results in an optimal cell movement and in an increment in membrane ruffling and in the formation of membrane-rich structures, such as lamellipodia, filopodia, indicative of a migratory phenotype (see Figure 4(B), upper inset).

Different studies have coherently shown that migration on planar substrates is limited for low fiber densities by the cells impossibility to form sufficient attachments to generate traction and to move forward [35, 44]. Optimal ligand densities, in contrast, that preclude the formation of stable focal adhesions [2, 12, 43, 57] but cause requires rapid focal adhesion turnovers, will result in maximal cell movement characterized by a migratory phenotype rich in migration-associated membrane protrusions. Eventually, at high densities migration is blocked because integrin receptors engage into stable focal adhesions that exclude coordinated attachment-detachment for cell movement [21, 30]. Blocked migration due to stable focal contact formation is usually accompanied by an increased spreaded area (again, refer to [12]), which we, however, did not capture with our approach.

3.5.2. *Cell-Fiber Adhesion Strength for 2D and 3D Matrices.* As integrin function impacts adhesion, we simulate cell motility both over 2D surfaces and within 3D matrices (at standard conditions, Fig. 1) as a function of varying cell-fiber adhesion strength ($J^{ext}_{C,F}$, which is the model counterpart of variations in integrin activation levels and affinity). As a basic migration-adhesion relationship, the migratory capability of moving individuals can be sorted into the three regimes of high, intermediate or low adhesion strength and in principle is valid for movements both over a surface or within a 3D matrix (Fig. 5). At high integrin engagement (say $J^{ext}_{C,F} < 3$), cells display barely no detectable movement within the observation

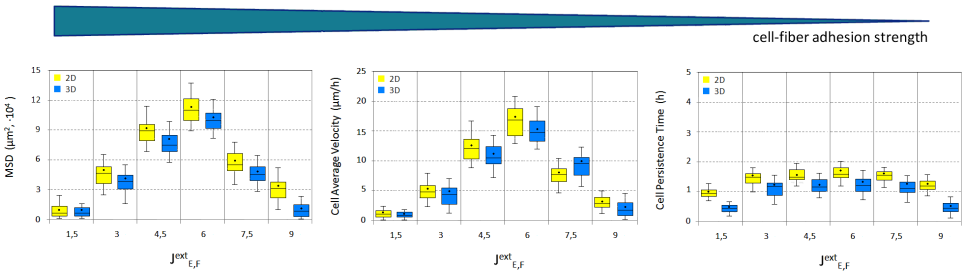

FIGURE 5. Biphasic relationship of cell motility and cell-fiber adhesion strength, given by the model parameter $J^{ext}_{C,F}$, for both 2D or 3D matrices. All other parameters remain unchanged, such as in the standard case of Fig. 1. The box-and-whisker plots (means are lines, medians are dots, see appendix) represent cell MSD, average velocity, and persistence time from 50 randomly selected cells. Maximal migratory capacity is seen at intermediate values of cell-fiber adhesiveness.

period, by being unable to detach from fibers. From an energetic view point, cells minimize the hamiltonian H by keeping such an adhesive contact. Given the high difference between $J^{ext}_{C,F}$ and $J^{ext}_{C,M}$, moving individuals have in fact no benefit from further movements, meaning that an overly adhesive substrate causes the formation of integrin clusters on the cell surface strongly binding to substrate and not allowing detachment as needed for further migration.

Intermediate values of $J^{ext}_{C,F}$ (say, in the interval [3,6]) yield moderately high adhesive forces associated with a balance of attachment and detachment, allowing cells to efficiently move along 2D surfaces or within the fibrous network with a maximal distance covered. Finally, above a certain value of $J^{ext}_{C,F}$ (say, > 6.5), adhesion is lacking, and consequently cells display barely detectable movement within the observation period. Given that $J^{ext}_{C,M} < J^{ext}_{C,F}$, cells prefer to fluctuate around the initial position in the interstitial fluid, avoiding contacts with the collagenous threads. Indeed, if a passive contact happens, cells soon detach from the fiber without exerting the traction needed for further movements.

The biphasic distribution of MSD is associated with a similar corresponding distribution in velocity, but only a flat curve in persistence, Figure 5. Therefore, the adhesion-dependent overall motility is mediated mostly by a cells velocity, whereas the persistent component of cell motion remains almost unaltered and refers to random movement (Figure 1(B)). In particular, persistence levels at < 1 at the lowest and highest $J^{ext}_{C,F}$ levels correspond with a running on the spot phenotype observed in experimental assays for cells embedded in matrix [84].

In both two and three dimensions, the similarity of the biphasic dependence between the migratory properties of cells and their adhesiveness are consistent with published experimental literature, i.e. on tumor cells expressing high levels of $\beta 1$ integrins [48]. However, they are not necessarily valid for all cell types, such as leukocytes that use adhesion-independent strategies when moving within a 3D collagen network [22]. The different assays used for cells when migrating on 2D or within 3D matrices have an impact on the conclusions of migration capacities. Whereas a non-adhesive cell detaches from a surface and cannot migrate anymore, non-adhesive cells are caught in a 3D network and may not, or may migrate by unspecific interactions with the lattice or by cytoskeleton-mediated propulsive mechanisms [24].

In accordance with our simulated data, a number of 3D ECM assays have shown similar trends for adherent cell types, such as human prostrate carcinoma cells, whose velocity has been plotted as a biphasic function of an adhesiveness parameter such as ligands functionality as well as receptor density [88], or melanoma cells, cultured in collagen scaffolds and stimulated with different concentrations of integrin-binding peptide RGD [10]. Finally, cell velocity can vary non-linearly with increasing ligand concentration, as it first increases, reaches a maximum and then decreases while the number of ligands still increase [47]. In summary, a medium level cell adhesion to underlying or surrounding ECM is of crucial importance for the effectiveness of cell migration.

3.6. **Fiber Elasticity of 3D Matrices.** In the body, extracellular tissues display a range of elastic characteristics that are modulated by the collagen content, the amount of cross-links between collagenous molecules and the presence of elastic fibers. Rigid tissues are usually dense and elastic tissues are often loose, and increasing matrix density will add rigidity. In experimental studies using 3D ECM that where either modulated in density, i.e., fiber concentration [85], or rigidity [55, 56, 72, 74], the other component becomes influenced as well. However, to separate the related effects, we here simulate both varying scaffold stiffness (regulated by ν_F) and the geometrical microstructure. To quantify such convoluting factors, we provide contour plots, as joint functions of pore size and fiber elasticity, that illustrate cell motile parameters as differently colored 'landscapes' (Fig. 6). It is useful to underline that elastic fibers are also characterized by a low constant $T_F = 0.2$, as they are no longer rigid but can deform.

In Fig. 6(A; top panels) at high pore size (i.e., 20 μm), cells display a reduced motile behavior, regardless of the fiber stiffness, as already shown in Fig. 3(A). The rationale of this is that in very loose tissues cells migration is not supported by fibers from all sides of the cell and consequently, the cell migrates along single fibers only that, however, when stiff, again promote to some extent traction and therefore migration. Next, at intermediate mesh dimensions, both cell velocity and persistence (and, consequently, the overall displacement) biphasically depend on matrix elasticity. If the collagenous threads are too elastic (i.e., $\nu_F < 3$), they can be easily deformed, without representing a sufficient anchor for pulling force generation required for cell motion. With a moderate stiffness (i.e., $5 < \nu_F < 9$), the matrix fibers can be slightly arranged to form contact-guidance cues, thereby facilitating cell migration. On the contrary, a too rigid network (i.e., $\nu_F > 9$) forms steric obstacles that can be somewhat less efficiently overcome by moving individuals. Finally, small pore sizes allow motility only within elastic matrices, whereas migration is negligible for intermediate or high rigidities of the fibers. Migrating cells are able to move within small pores in fact only by significantly deforming the matrix network, creating open space to pass through. Therefore, if the pore size is much smaller than cell dimension, the mechanical matrix characteristics exert an increasing influence. When evaluating the plots at constant rigidity, cell migration displays the same bimodal dependence on pore size previously captured in Fig. 3(A).

Such variations in fiber rigidity induce a suite of cell morphological changes (Fig. 7). Cells plated within rigid scaffolds are typically well elongated and exhibit multiple fiber-associated constrictions along their bodies. They indeed adapt their shape and squeeze through rigid matrix arrangements by concomitant elongation of their body. Cells cultured in progressively soft matrices show instead decreasing

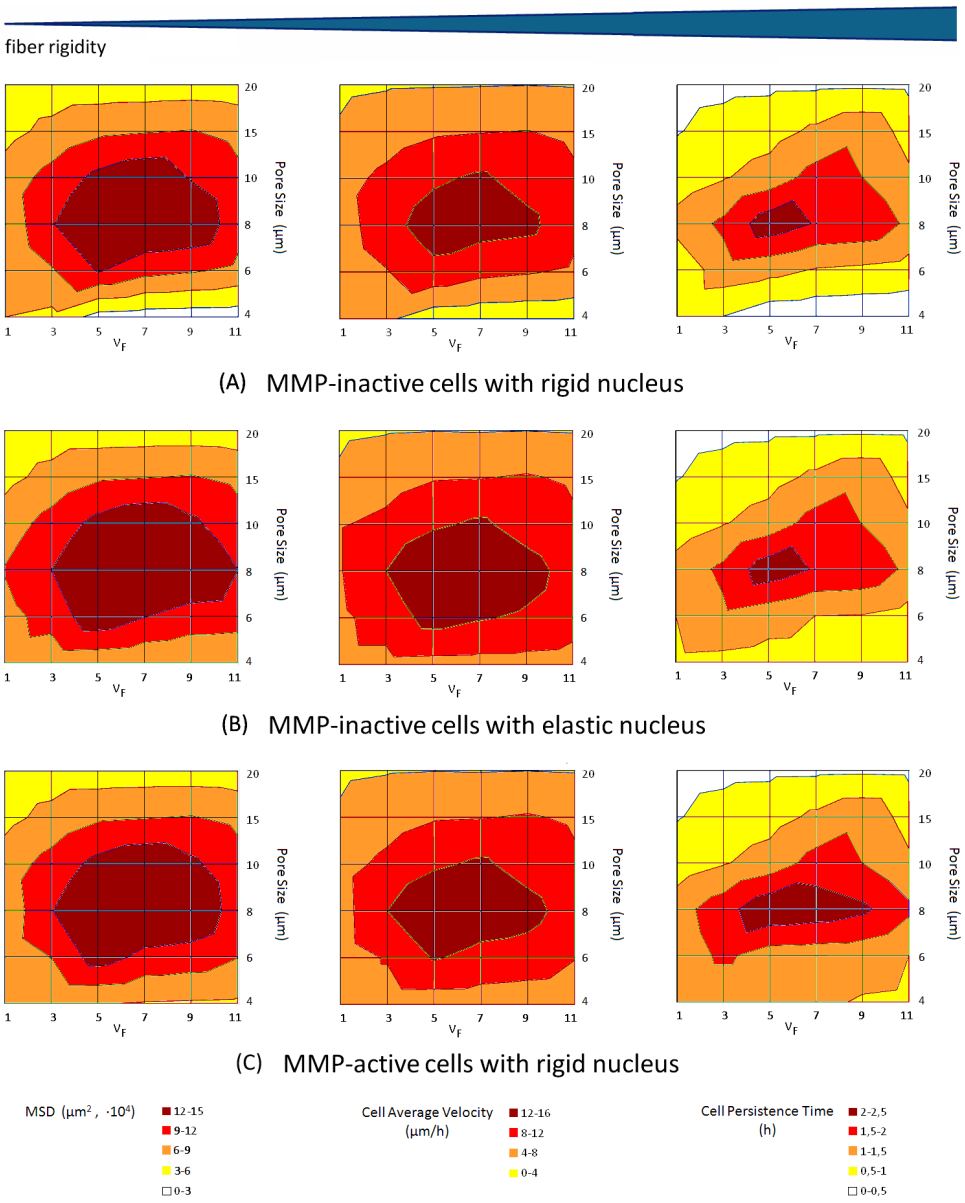

FIGURE 6. 3D cell migration as a function of fiber rigidity ν_F and pore size. Contour plots of cell migratory parameters for (A) standard conditions (see Figure 1), that further includes the absence of proteolytic activity and a stiff nucleus ($\nu_N = 8.5$), (B) cells as in (A) but with an elastic nucleus ($\nu_N = 0.5$) and (C) cells as in (A) but expressing matrix degrading enzymes, regulated by Eq. (7). Each value is given as mean over 50 randomly chosen individuals (see appendix).

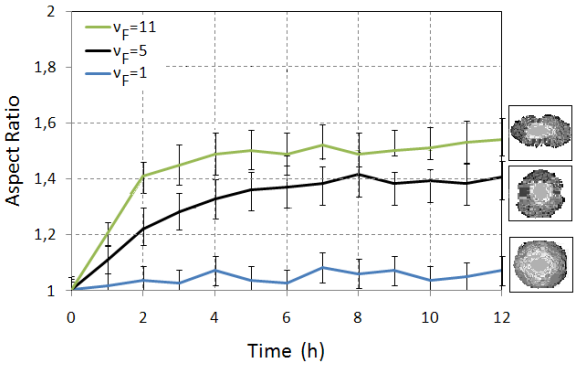

FIGURE 7. Dependency of cell deformation on fiber stiffness. Variations of cells aspect ratio (defined as in Figs. 3 and 4) during migration at different fiber elasticities: from bottom to top $\nu_F = 1, 5, 11$. In particular, the pore size is kept at 5 μm.

elongation, and cells within complete compliant ECMs remain uniformly rounded, as they easily deform the collagen-like threads and lack cytoskeletal traction [79]. In summary, cells migrate in a biphasic manner at theoretic conditions of either increasing density or increasing stiffness alone, but, however, also at experimental conditions, upon combined increase of density and stiffness together (imagine a decreasing curve in the plots of Fig.6 from left top to right bottom).

As experimental examples, bimodal relationships between cell migratory ability and the deformability of 3D matrix scaffolds have been observed in experimental models of smooth muscle cells [59] and mouse fibroblasts, cultured in stepwise EDAC-cross-linked CG matrices of constant pore size [37]. A biphasic dependence on matrix rigidity has been previously reported also in isotropic homogeneous networks, as in the case of prostate cancer cells embedded in Matrigel with a fixed fibronectin level and variables stiffness [88].

3.7. **Nuclear Compressibility in 3D Migration.** As pointed out in the previous section, to migrate within ECM of pores smaller than a cellular diameter, cells need to deform their body including their nucleus, as the most rigid organelle [26]. The degree of nuclear deformability therefore may contribute to the migration efficiency of a cell. The nucleus elasticity is mainly regulated by both the chromatin structure, and lamin intermediate filaments, that form a part of the nuclear envelope, [26, 31]. The softness of a nucleus can be modeled by lowering the values of the nuclear rigidity ν_N from 8.5 (see Table 1) to 0.5 (compare Fig. 6(A) and (B)). At high pore size of 10 μm or higher and lower fiber rigidity (i.e., at left upper corner), migration remains unaltered regardless of nuclear elasticity, as moving cells do not experience steric hindrance. However, once mesh dimensions and scaffold rigidity move to a intermediate ranges, nuclear elasticity somewhat facilitates cell movement, measured as MSD (an estimate product of persistence time and velocity). Whereas the persistence time does not contribute to this increase (i.e., cells with rigid nuclei were already able to migrate through the matrix networks characterized by intermediate dimensions without changing direction), the velocity does (i.e., they can quickly and efficiently remodel). Finally, as pore size and matrix elasticity further decrease towards a highly constrained environment (lower right

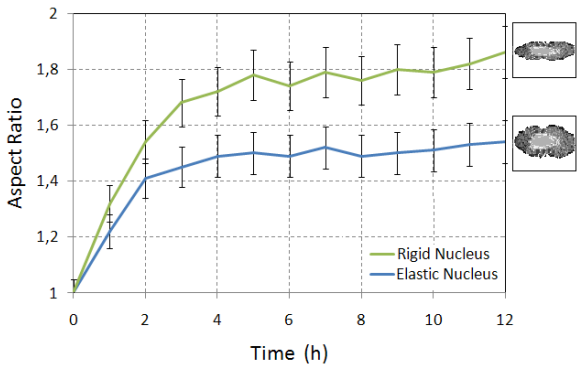

FIGURE 8. Dependence of migration-associated cell morphology over time on nuclear deformability. Evolution of cells aspect ratio during migration trough small pore sizes (i.e., 5 μm) and high fiber stiffness (i.e., $\nu_F = 11$). Green line represents cells with a standard rigid nucleus ($\nu_N = 8.5$), blue line represents cells with an elastic nucleus ($\nu_N = 0.5$). All the other model parameters are the same as the standard simulation of Fig. 1. Note that a high deformability of the nucleus allows cells to undergo dramatic morphological transitions, fundamental for their migration in highly constrained environments.

corner), the simulations demonstrate that enhanced nuclear deformability is associated with enhanced cell migration. Such facilitated locomotion is mediated by an elongated and deformable nuclear configuration allowing the entire cell to squeeze and stretch more easily and thereby pass through the steric obstacles of a dense and rigid matrix (Fig. 8).

Our simulations relate to a number of experimental works, such as [81], where cell migration efficiency decreases with matrix density and is associated with nuclear deformation, or [6], where glioma cell lines significantly deform their nucleus upon recruitment of non-muscle myosin II (NMMII) for squeezing through narrow locations in a brain model *in vivo*, thereby increasing their metastatic potential.

3.8. **Matrix Degradation in 3D Migration.** In the previous sections, we have demonstrated that cells move within matrix fibers of varying density and stiffness, that act as constraints, deforming both body and nucleus. As an additional mechanism to overcome limited space cells may upregulate proteolytic enzymes that degrade ECM structure (i.e., matrix metalloproteinases, MMPs) that act either bound to the cell surface or when secreted into the extracellular space. Accordingly, cells degrade steric fiber obstacles either in a cell contact-dependent manner targeting locally confining fibers, or, in a diffusive manner leading to gradient formation and consequently, a more overall weakening of the surrounding tissue structure [83]. As a result, barrier-free matrix spaces will be created resulting in longer distance traveling. We here perform simulations with cells that execute both contact-dependent and soluble proteolysis. The local concentration of the net protolytic activity (both surface-bound or diffusive) is defined as $m(\mathbf{x}, t)$, and is assumed to evolve following

a standard reaction-diffusion equation:

$$\frac{\partial m(\mathbf{x},t)}{\partial t} = \underbrace{P(\mathbf{x},t)}_{production} + \underbrace{D_m \nabla^2 m(\mathbf{x},t)}_{diffusion} - \underbrace{\lambda_m m(\mathbf{x},t)\delta(\tau(\Sigma_{\sigma(\mathbf{x})}),M)}_{decay}, \tag{7}$$

where $\delta(\tau(\Sigma_{\sigma(\mathbf{x})}),M) = 1$ in the interstitial medium M and 0 elsewhere. λ_m and D_m are, respectively, the decay rate and the effective diffusion coefficient of proteolytic enzymes, constant and homogeneous in the extracellular environment. A low value of D_m models proteolysis being strongly localized in regions close to cell membranes, in agreement with experimental evidence in [68, 81]. $P(\mathbf{x},t)$ models instead the local production of proteases either at the cell surface or secreted away from the external cell surface, at a constant rate π_m collagenous component:

$$P(\mathbf{x},t) = \begin{cases} \pi_m & \text{if} \quad \mathbf{x} : \tau(\Sigma_{\sigma(\mathbf{x})}) = C \quad \text{and} \quad \exists \mathbf{x}' \in \Omega_{\mathbf{x}}^{'} \ : \ \tau(\Sigma_{\sigma(\mathbf{x}')}) = M; \\ 0 & \text{else}, \end{cases} \tag{8}$$

where we recall that C stands for cell cytosolic region. MMPs are capable to degrade the fibrous component of the matrix: to reproduce this biological effect, a lattice grid site $\mathbf{x}$ belonging to a degraded collagenous fiber becomes a generalized medium (fluid) site when its local level of MMPs ($m(\mathbf{x},t)$) is sufficiently high (in our simulations above 2.5 μM). This change is implemented by changing its type τ from F (fiber) to M (medium), as done in [32]. The comparison of cell migration of either MMP-active and MMP-inactive individuals (Fig. 6(A) and (C)), reveals that at high and intermediate pore size and/or low matrix rigidity, the proteolytic machinery does not appreciably affect cell motion. The loose fiber network does not represent a significative obstacle for cell migration, which therefore is not enhanced further by MMP activity. In the case of small pores formed by rigid collagenous fibers (lower right), MMP activity promotes instead appreciable cell migration. This suggests that proteases, by degrading matrix fibers, are able to break steric obstacles in the close proximity of moving individuals, opening spaces for them to sample greater distances without turning back.

The role of MMPs activity in cell migratory behavior captured in our model is in good agreement with the experimental results provided in [62] for dermal fibroblasts embedded in molecularly engineered PEG hydrogels, where a significative increment in the number of migrating individuals was observed upon up-regulation of proteolytic enzymes.

In conclusion, summarizing all the examined parameters, cell migration is greatly influenced by a number of complex ECM- and cell-derived characteristics that, in addition, display a number of interdependencies [28] and, together, determine the net outcome on migration.

4. **Discussion.** Due to the increasingly recognized importance of cell migration processes in matrix environments and its exploitation for therapy and for tissue engineering, an increasing number of theoretical models have been developed. These modeling approaches analyze the relative importance of single and interrelated parameters to predict migration behavior.

We employed a simple and intuitive version of the Cellular Potts Model to simulate the motile behavior of cells seeded either on two-dimensional matrix substrates or embedded within three-dimensional matrix scaffolds. In contrast to previous

approaches, the Cellular Potts Model used here treats each cell physical object compartmentalized into nucleus and cytoplasm, whose movement is driven by explicit interactions with the extracellular, environment in turn differentiated into fibers and medium. The introduction of the nucleus and its mechanical properties on one side and of the extracellular matrix and its specific fibrous characteristics on the other side allowed to simulate for the first time both their specific contributions in cell migration.

In particular, we considered isolated pro-migratory parameters derived either from the ECM, such as orientation, pore size, ligand density, or rigidity, or from the cell, such as adhesion, nuclear rigidity, or proteolysis, that control both cell migration efficiency and migratory phenotypes. In all proposed cases, the computational results are consistent with a number of published experimental counterparts, and represent further complementary determinations. For instance, we have provided evidence that cell maximal dispersion occurs at intermediates fiber densities, i.e in matrices with a fiber mesh of an optimal size for a cell to spread (in 2D) or to squeeze through (in 3D). Indeed, if the inter-fiber distance becomes too wide, moving cells loose the availability of anchorage points and the contact guidance necessary for traction and further movement. On the contrary, if planar matrices have a too high concentration of collagenous fibers, moving individual loose their preference for the fibrous component of the substrate, displaying limited movement. In 3D, if the fiber network is formed by small pores, cells can not pass through, since their nucleus is not able to sufficiently deform. The presented approach has also demonstrated that cell migratory behavior has a biphasic dependence on the strength of cell-fiber attachment, with maximal values at intermediate adhesive interactions in both dimensionalities. We have then more carefully focused on how microstructural properties of 3D scaffolds, not widely considered central to 2D motility, influence the overall cell motile phenotype. Indeed, the model has highlighted the complex dependency of cell motility on the matrix elastic modulus. Specifically, at intermediate pore size, higher level of cell migratory capacity was observed in moderately rigid scaffolds, while at small pore dimensions, cell movement has been restricted only in the softest matrix (i.e., characterized by highly deformable fibers). At big pore measures, the rigidity of the collagenous threads has not been observed to influence cell locomotion. Finally, we have clearly shown that significant cell movement through highly constrained environments can only be achieved through a combination of proteolytic degradation of the matrix and/or an enhancement contractility of cell nucleus.

As a clear advantage of a theoretical approach, we have been able to independently vary and modulate in a graded fashion all biophysical cell parameters and microstructural properties of the matrix environment, which is helpful in dissecting the complex relationships between cell motility and the biophysical, biochemical and molecular properties of the matrix [28]. However, a modeling approach that describes isolated parameters is unable to encompass the complexity apparent in processes *in vivo*, such as cancer invasion. Some of these additional, here disregarded, factors are (i) additional matrix deposition of moving individuals, leading to altered traction generation, adhesion and contact guidance; (ii) soluble or matrix-bound gradients of chemoattractants; (iii) molecular signals transmitted from the ECM to cells (outside-in signaling), thereby changing the activity of polarization- or contractility-mediating proteins (Rac, Rho) [24]; or (iv) inside-out signaling for reinforcement of adhesion [79].

Despite the limitations of theoretical modeling, our approach could be applied to the design of synthetic implant materials, i.e., a cellular scaffolds with optimal values of pore size and stiffness that may accelerate cell in-growth, critically for regenerative treatments [7, 11, 38, 80]. Further, applying the proposed model on defined cancer invasion models and inhibitory strategies may assist to predict the outcome on therapeutic interventions. At this regard, it would be biologically relevant to adapt our approach to specific cell lines, characterized by distinct biophysical phenotypes (i.e., intrinsic motility, elasticity, or proteases activity). This can be easily done by inheriting the model parameters from experimentally-measured quantities, characteristic of the selected cell population. It would be also interesting to analyze collective migrations of cellular ensembles both of the same type or of different types, which are fundamental in several physio-pathological processes, as commented in [39]. A differentiation may in fact occur among individuals of the same family (i.e., tip and stalk cells during angiogenic processes, or leader and follower cells during a skin wound healing [29]), whereas competitions for nutrients or altered heterotypic interactions may significantly affect the migratory capacity of an entire cell lineage (for example, cancer cells of epithelial origin inhibit the motility and induce apoptosis in neighboring normal individuals). Obviously, in this case, it is necessary to define in the model framework all cell types, with the relative phenotypic parameters and the rules for their behavior and mutual interactions.

In summary, our findings may contribute to both understanding and exploitation of cell migration processes on and in tissues.

Appendix A. **Appendix.** The *position* at time t of a cell η is established by the coordinate of its center of mass (CM) $\mathbf{x}_\eta^{CM}(t)$. The wind-rose plots in both the two- and in the three-dimensional case are therefore generated by tracking the position of the center of mass of 10 randomly chosen cells at 15-min (450 MCS) intervals, overlying the starting coordinates at the origin of the graph. This type of representation is particularly useful to evaluate the cell net displacements over time and the distribution of their final dispersion.

Similarly, the *instantaneous velocity* of η is the instantaneous velocity of its center of mass:

$$\mathbf{v}_\eta(t) = \frac{\mathbf{x}_\eta^{CM}(t) - \mathbf{x}_\eta^{CM}(t-\Delta t)}{\Delta t}, \tag{9}$$

where $\Delta t = 1$ MCS, as done in similar works [51, 58, 70].

The *average velocity* of an individual over the entire simulation is instead given by

$$\overline{\mathbf{v}}_\eta(t) = \frac{\mathbf{x}_\eta^{CM}(t_{final}) - \mathbf{x}_\eta^{CM}(0)}{t_{final}}, \tag{10}$$

where t_{final} corresponds to the final time of the observation period which, as explained in the text, is set to 21600 MCS (12 hours).

The *mean squared displacement* (MSD) at time t of a cell η, defined as $< d^2(t) >$, is calculated as

$$< d_\eta^2(t) > = < (\mathbf{x}_\eta^{CM}(t) - \mathbf{x}_\eta^{CM}(0))^2 >, \tag{11}$$

where $\mathbf{x}_\eta^{CM}(0)$ is the initial position of its center of mass. Following [16, 87], the squared displacements are averaged over all previous time steps, in order to take into account the back and forth motions exhibited by the moving individuals. As demonstrated in a number of previous experimental [16, 37] and computational

[16, 87] studies, at sufficiently long times the mean square displacements vary approximately linearly with the number of time steps. It can therefore be related to cell *instantaneous velocity* ($\mathbf{v}_\eta$) and *persistence time* (p_η, which quantifies the directional productive motion) with the so-called *persistence-random-walk* (PRW) law:

$$< d_\eta^2(t) >= 2\mathbf{v}_\eta^2(t)p_\eta(t)[t - p_\eta(t)(1 - e^{-t/p_\eta(t)})]. \tag{12}$$

In particular, at still longer observation periods, (12) reduces to:

$$< d_\eta^2(t) >\approx 2\mathbf{v}_\eta^2(t)p_\eta(t)t, \tag{13}$$

and the persistence time of a moving individual can be directly calculated as

$$p_\eta(t) \approx \frac{< d_\eta^2(t) >}{2\mathbf{v}_\eta^2(t)t}. \tag{14}$$

The PRW relation has been demonstrated to characterize the cells migratory behavior more properly than other common methods, which calculate the average distance migrated by biological individuals in an arbitrary time interval, as commented in [20]. For the statistical analysis, cells that do not display a final MSD greater than their diameters are classified as non-motile and assigned a velocity of 0 μm/h and an undefined persistence time, as we follow the criterion described in [16, 30].

A.1. **Statistics.** Cell motile parameters (MSD, velocity and persistence time) are represented in the figures as box-and-whisker plots, where the edges of the boxes are the 25^{th} and 75^{th} percentiles and the whiskers the 10^{th} and 90^{th} percentiles. The horizontal line represents the median, while the large black dot corresponds to the mean of the distribution. Statistical significance ($p < 0.05$) was determined for motile fraction data by the Students' t-test and for non-normally distributed data sets by the Kolmogorov-Smirnov test over each 50 randomly chosen individuals.

In the multidimensional contour plots the values of the cell migratory parameters are means over 50 randomly chosen individuals.

Quantitative analysis of cell morphological changes is carried out by evaluating the evolution of the cell *aspect ratio*, given by the ratio between the actual cell surface (respectively, perimeter in 2D) and the surface of the sphere having the same volume (respectively, the perimeter of the circle having the same area in 2D). It is useful to underline that in our model cell volume (respectively, area in 2D) is kept nearly fixed by high values of κ in Eq. (4), see Table 1. Therefore the aspect ratio gives a quantitative measure of cell membrane ruffling. Finally, the time evolution of the aspect ratio is given in the plots with mean $\pm$ s.d. over 50 randomly chosen individuals.

Acknowledgements. We would like to thank the referees very much for their valuable comments and suggestions.

REFERENCES

[1] B. Alberts, D. Bray, J. Lewis, M. Raff, K. Roberts and J. D. Watson, "Molecular Biology of the Cell," 3^{rd} edition, Garland Science, 1994.

[2] M. Arnold, V. C. Hirschfeld-Warneken, T. Lohmüller, P. Heil, J. Blümmel, E. A. Cavalcanti-Adam, M. López-García, P. Walther, H. Kessler, B. Geiger and J. P. Spatz, *Induction of cell polarization and migration by a gradient of nanoscale variations in adhesive ligand spacing*, Nano Lett., **8** (2008), 2063–2069.

[3] M. Bajénoff, J. G. Egen, L. Y. Koo, J. P. Laugier, F. Brau, N. Glaichenhaus and R. N. Germain, *Stromal cell networks regulate lymphocyte entry, migration, and territoriality in lymph nodes*, Immunity, **25** (2006), 989–1001.

[4] A. Balter, R. M. Merks, N. J. Poplawski, M. Swat and J. A. Glazier, *The Glazier-Graner-Hogeweg model: Extensions, future directions, and opportunities for further study*, in "Single-Cell-Based Models in Biology and Medicine, Mathematics and Biosciences in Interactions" (eds. A. R. A. Anderson, M. A. J. Chaplain and K. A. Rejniak), Birkhaüser, (2007), 157–167.

[5] A. L. Bauer, T. L. Jackson and Y. Jiang, *A cell-based model exhibiting branching and anastomosis during tumor-induced angiogenesis*, Biophys. J., **92** (2007), 3105–3121.

[6] C. Beadle, M. C. Assanah, P. Monzo, R. Vallee, S. Rosenfeld and P. Canoll, *The role of myosin ii in glioma invasion of the brain*, Mol. Biol. Cell., **19** (2008), 3357-3368.

[7] J. Behring, R. Junker, X. F. Walboomers, B. Chessnut and J. A. Jansen, *Toward guided tissue and bone regeneration: morphology, attachment, proliferation, and migration of cells cultured on collagen barrier membranes. A systematic review*, Odontology, **96** (2008), 1-11.

[8] A. O. Brightman, B. P. Rajwa, J. E. Sturgis, M. E. McCallister, J. P. Robinson and S. L. Voytik-Harbin, *Time-lapse confocal reflection microscopy of collagen fibrillogenesis and extracellular matrix assembly in vitro*, Biopolymers, **54** (2000), 222-234.

[9] A. Brock, E. Chang, C. C. Ho, P. LeDuc, X. Jiang, G. M. Whitesides and D. E. Ingber, *Geometric determinants of directional cell motility revealed using microcontact printing*, Langmuir, **19** (2003), 1611-1617.

[10] B. T. Burgess, J. L. Myles and R. B. Dickinson, *Quantitative analysis of adhesion-mediated cell migration in three-dimensional gels of RGD-grafted collagen*, Ann. Biomed. Eng., **28** (2003), 110-118.

[11] R. M. Capito and M. Spector, *Scaffold-based articular cartilage repair*, IEEE Eng. Med. Biol. Mag., **22** (2003), 42 - 50.

[12] E. A. Cavalcanti-Adam, T. Volberg, A. Micoulet, H. Kessler, B. Geiger and J. P. Spatz, *Cell spreading and focal adhesion dynamics are regulated by spacing of integrin ligands*, Biophys. J., **92** (2007), 2964–2974.

[13] J. Condeelis and J. E. Segall, *Intravital imaging of cell movement in tumours*, Nat. Rev. Cancer, **3** (2003), 921-930.

[14] M. W. Conklin, J. C. Eickhoff, K. M. Riching, C. A. Pehlke, K. W. Eliceiri, P. P. Provenzano, A. Friedl and P. J. Keely, *Aligned collagen is a prognostic signature for survival in human breast carcinoma*, Am. J. Pathol., **178** (2011), 1221-1232.

[15] R. B. Dickinson, S. Guido and R. T. Tranquillo, *Biased cellmigration of fibroblasts exhibiting contact guidance in oriented collagen gels*, Ann. Biomed. Eng., **22** (1994), 342 - 356.

[16] P. A. DiMilla, J. A. Stone, J. A. Quinn, S. M. Albelda and D. A. Lauffenburger, *Maximal migration of human smooth-muscle cells on fibronectin and type-IV collagen occurs at an intermediate attachment strength*, J. Cell. Biol., **122** (1993), 729-737.

[17] A. D. Doyle, F. W. Wang, K. Matsumoto and K. M. Yamada, *One-dimensional topography underlies three-dimensional fibrillar cell migration*, J. Cell. Biol., **184** (2009), 481-490.

[18] N. Dubey, P. C. Letourneau and R. T. Tranquillo, *Neuronal contact guidance in magnetically aligned fibrin gels: effect of variation in gel mechano-structural properties*, Biomaterials, **22** (2001), 1065-1075.

[19] G. A. Dunn and T. Ebendal, *Contact guidance on oriented collagen gels*, Exp. Cell. Res., **111** (1978), 475-479.

[20] G. A. Dunn, *Characterizing a kinesis response: time-averaged measures of cell speed and directional persistence*, Agents Actions Suppl., **12** (1983), 14–33.

[21] A. Engler, L. Bacakova, C. Newman, A. Hategan, M. Griffin and D. Discher, *Substrate compliance versus ligand density in cell on gel responses*, Biophys. J., **86** (2004), 617-628.

[22] P. Friedl, F. Entschladen, C. Conrad, B. Niggemann and K. S. Zänker, *CD4+ T-lymphocytes migrating in three-dimensional collagen lattices lack focal adhesions and utilize β1 integrin-independent strategies for polarization, interaction with collagen fibers and locomotion*, Eur. J. Immunol., **28** (1998), 2331–2343.

[23] P. Friedl and E. B. Brocker, *The biology of cell locomotion within three-dimensional extracellular matrix*, Cell. Mol. Life Sci., **57** (2000), 41-64.

[24] P. Friedl and K. Wolf, *Tumour-cell invasion and migration: diversity and escape mechanisms*, Nat. Rev. Cancer, **3** (2003), 362-374.

[25] P. Friedl, K. Maaser, C. E. Klein, B. Niggemann, G. Krohne and K. S. Zänker, *Migration of highly aggressive MV3 melanoma cells in 3-dimensional collagen lattices results in local*

matrix reorganization and shedding of alpha2 and beta1 integrins and CD44, Cancer Res., **57** (1997), 2061–2070.

[26] P. Friedl, K. Wolf and J. Lammerding, *Nuclear mechanics during cell migration*, Curr. Opin. Cell. Biol., **23** (2011), 253.

[27] P. Friedl and B. Weigelin, *Interstitial leukocyte migration and immune function*, Nat. Immunol., **9** (2008), 960-969.

[28] P. Friedl and K. Wolf, *Plasticity of cell migration: a multiscale tuning model*, J. Cell. Biol., **188** (2009), 11-19.

[29] P. Friedl and D. Gilmour, *Collective cell migration in morphogenesis, regeneration and cancer*, Nat. Rev. Mol. Cell. Biol., **10** (2009), 445–457.

[30] C. Gaudet, W. Marganski, S. Kim, C. T. Brown, V. Gunderia, M. Dembo and J. Wong, *Influence of type I collagen surface density on fibroblast spreading, motility, and contractility*, Biophys. J., **85** (2003), 3329-3335.

[31] G. Gerlitz and M. Bustin, *The role of chromatin structure in cell migration*, Trends Cell. Biol., **21** (2011), 6–11.

[32] C. Giverso, M. Scianna, L. Preziosi, N. Lo Buono and A. Funaro, *Individual cell-based model for in-vitro mesothelial invasion of ovarian cancer*, Math. Model. Nat. Phenom., **5** (2010), 203–223.

[33] J. A. Glazier, A. Balter and N. J. Poplawski, *Magnetization to morphogenesis: A brief history of the Glazier-Graner-Hogeweg model*, in "Single-Cell-Based Models in Biology and Medicine, Mathematics and Biosciences in Interactions" (eds. A. R. A. Anderson, M. A. J. Chaplain and K. A. Rejniak), Birkhaüser, (2007), 79–106.

[34] J. A. Glazier and F. Graner, *Simulation of the differential adhesion driven rearrangement of biological cells*, Phys. Rev. E Stat. Phys. Plasmas Fluids Relat. Interdiscip. Topics, **47** (1993), 2128-2154.

[35] S. L. Goodman, G. Risse and K. Vondermark, *The E8 subfragment of laminin promotes locomotion of myoblasts over extracellular- matrix*, J. Cell. Biol., **109** (1989), 799-809.

[36] F. Graner and J. A. Glazier, *Simulation of biological cell sorting using a two-dimensional extended Potts model*, Phys. Rev. Lett., **69** (1992), 2013–2016.

[37] B. A. Harley, H. Kim, M. H. Zaman, I. V. Yannas, D. A. Lauffenburger and L. J. Gibson, *Microarchitecture of three-dimensional scaffolds influences cell migration behavior via junction interactions*, Biophys. J., **95** (2008), 4013-4024.

[38] B. A. Harley, M. H. Spilker, J. W. Wu, K. Asano, H. P. Hsu, M. Spector and I. V. Yannas, *Optimal degradation rate for collagen chambers used for regeneration of peripheral nerves over long gaps*, Cells Tissues Organs, **176** (2008), 153-165.

[39] O. Ilina and P. Friedl, *Mechanisms of collective cell migration at a glance*, J. Cell Sci., **122** (2009), 3203–3208.

[40] E. Ising, *Beitrag zur theorie des ferromagnetismus*, Z. Physik., **31** (1925), 253.

[41] R. M. Kuntz and W. M. Saltzman, *Neutrophil motility in extracellular matrix gels: mesh size and adhesion affect speed of migration*, Biophys. J., **72** (1997), 1472-1480.

[42] S. Kurosaka and A. Kashina, *Cell biology of embryonic migration*, Birth Defects Res. C. Embryo Today, **84** (2008), 102-122.

[43] E. Lamers, R. Van Horssen, J. Te Riet, F. C. Van Delft, R. Luttge, X. F. Walboomers and J. A. Jansen, *The influence of nanoscale topographical cues on initial osteoblast morphology and migration*, Eur. Cell. Mater., **9** (2010), 329–343.

[44] D. A. Lauffenburger and J. J. Lindermann, "Receptors: bodels for binding, trafficking, and signaling," Oxford University Press, London, 1996.

[45] D. A. Lauffenburger and A. F. Horwitz, *Cell migration: a physically integrated molecular process*, Cell, **84** (1996), 359-369.

[46] D. Lehnert, B. Wehrle-Haller, C. David, U. Weiland, C. Ballestrem, B. A. Imhof and M. Bastmeyer, *Cell behaviour on micropatterned substrata: limits of extracellular matrix geometry for spreading and adhesion*, J. Cell. Sci., **117** (2004), 41-52.

[47] M. P. Lutolf, J. L. Lauer-Fields, H. G. Schmoekel, A. T. Metters, F. E. Weber, G. B. Fields and J. A. Hubbell, *Synthetic matrix metalloproteinase-sensitive hydrogels for the conduction of tissue regeneration: engineering cell-invasion characteristics*, Proc. Natl. Acad. Sci. U. S. A., **100** (2003), 5413-5418.

[48] K. Maaser, K. Wolf, C. E. Klein, B. Niggemann, K. S. Zänker, E. B. Bröcker and Friedl, *Functional hierarchy of simultaneously expressed adhesion receptors: integrin $\alpha 2\beta 1$ but not CD44*

mediates MV3 melanoma cell migration and matrix reorganization within three-dimensional hyaluronan-containing collagen matrices, Mol. Biol. Cell., **10** (1999), 3067–3079.

[49] A. W. Mahoney, B. G. Smith, N. S. Flann and G. J. Podgorski, *Discovering novel cancer therapies: A computational modeling and search approach*, in "IEEE conference on Computational Intelligence in Bioinformatics and Bioengineering," (2008), 233-240.

[50] A. F. M arée, V. A. Grieneisen and P. Hogeweg, *The Cellular Potts Model and biophysical properties of cells, tissues and morphogenesis*, in "Single-Cell-Based Models in Biology and Medicine, Mathematics and Biosciences in Interactions" (eds. A. R. A. Anderson, M. A. J. Chaplain and K. A. Rejniak), Birkhaüser, (2007), 107–136.

[51] R. M. Merks, E. D. Perryn, A. Shirinifard and J. A. Glazier, *Contact-inhibited chemotaxis in de novo and sprouting blood vessel growth*, PLoS Comput. Biol., **4** (2008), e1000163, 16 pp.

[52] N. Metropolis, A. W. Rosenbluth, M. N. Rosenbluth, A. H. Teller and E. Teller, *Equation of state calculations by fast computing machines*, J. Chem. Phys., **21** (1953), 1087-1092.

[53] A. Mogilner and G. Oster, *Polymer motors: pushing out the front and pulling up the back*, Current Biology, **13** (2003), R721-R733.

[54] F. J. O'Brien, B. A. Harley, I. V. Yannas and L. Gibson, *Influence of freezing rate on pore structure in freeze-dried collagen-GAG scaffolds*, Biomaterials, **25** (2004), 1077-1086.

[55] L. H. Olde Damink, P. J. Dijkstra, M. J. Luyn, P. B. Wachem, P. Nieuwenhuis and J. Feijen, *Glutaraldehyde as a crosslinking agent for collagen-based biomaterials*, J. Mater. Sci. Mater. Med., **6** (1995), 460-472.

[56] J. M. Orban, L. B. Wilson, J. A. Kofroth, M. S. El-Kurdi, T. M. Maul and D. A. Vorp, *Crosslinking of collagen gels by transglutaminase*, J. Biomed. Mater. Res. A, **68** (2004), 756-762.

[57] S. P. Palecek, J. C. Loftus, M. H. Ginsberg, D. A. Lauffenburger and A. F. Horwitz, *Integrin-ligand binding properties govern cell migration speed through cell-substratum adhesiveness*, Nature, **385** (1997), 537-540.

[58] E. D. Perryn, A. Czirok and C. D. Little, *Vascular sprout formation entails tissue deformations and VE-cadherin-dependent cell-autonomous motility*, Dev. Biol., **313** (2008), 545–555.

[59] S. R. Peyton and A. J. Putnam, *Extracellular matrix rigidity governs smooth muscle cell motility in a biphasic fashion*, J. Cell. Physiol., **204** (2005), 198-209.

[60] T. D. Pollard and G. G. Borisy, *Cellular motility driven by assembly and disassembly of actin filaments*, Cell, **112** (2003), 453-465.

[61] R. B. Potts, *Some generalized order-disorder transformations*, Proc. Camb. Phil. Soc., **48** (1952), 106–109.

[62] G. P. Raeber, M. P. Lutolf and J. A. Hubbell, *Molecularly engineered PEG hydrogels: a novel model system for proteolytically mediated cell migration*, Biophys. J., **89** (2005), 1374-1388.

[63] C. B. Raub, V. Suresh, T. Krasieva, J. Lyubovitsky, J. D. Mih, A. J. Putnam, B. J. Tromberg and S. C. George, *Noninvasive assessment of collagen gel microstructure and mechanics using multiphoton microscopy*, Biophys. J., **92** (2007), 2212-2222.

[64] A. J. Ridley, M. A. Schwartz, K. Burridge, R. A. Firtel, M. H. Ginsberg, G. Borisy, J. T. Parsons and A. R. Horwitz, *Cell migration: integrating signals from front to back*, Science, **302** (2003), 1704-1709.

[65] B. A. Roeder, K. Kokini, J. E. Sturgis, J. P. Robinson and S. L. Voytik-Harbin, *Tensile mechanical properties of three-dimensional type I collagen extracellular matrices with varied microstructure*, J. Biomech. Eng., **124** (2002), 214-222.

[66] C. G. Rolli, T. Seufferlein, R. Kemkemer and J. P. Spatz, *Impact of tumor cell cytoskeleton organization on invasiveness and migration: a microchannel-based approach*, PLoS ONE, **5** (2010), e8726.

[67] B. M. Rubenstein and L. J. Kaufman, *The role of extracellular matrix in glioma invasion: a Cellular Potts Model Approach*, Biophys. J., **95** (2006), 5661–5680.

[68] F. Sabeh, R. Shimizu-Hirota and S. J. Weiss, *Protease-dependent versus -independent cancer cell invasion programs: three-dimensional amoeboid movement revisited*, J. Cell. Biol., **185** (2009), 11–19.

[69] E. Sahai, *Illuminating the metastatic process*, Nat. Rev. Cancer, **7** (2007), 737-749.

[70] M. Scianna, *A multiscale hybrid model for pro-angiogenic calcium signals in a vascular endothelial cell*, Bull. Math. Biol., **76** (2011), 1253–1291.

[71] M. Scianna and L. Preziosi, *Multiscale developments of the Cellular Potts Model*, Multiscale Model. Simul., **10** (2012), 342–382.

[72] M. T. Sheu, J. C. Huang, G. C. Yeh and H. O. Ho, *Characterization of collagen gel solutions and collagen matrices for cell culture*, Biomaterials, **22** (2001), 1713-1719.

[73] S. Schmidt and P. Friedl, *Interstitial cell migration: integrin-dependent and alternative adhesion mechanisms*, Cell. Tissue Res., **339** (2010), 83–92.

[74] R. C. Siegel, *Collagen cross-linking. Synthesis of collagen cross-links in vitro with highly purified lysyl oxidase*, J. Biol. Chem., **251** (1976), 5786-5792.

[75] C. Spadaccio, A. Rainer, S. De Porcellinis, M. Centola, F. De Marco, M. Chello, M. Trombetta, M. and J. A. Genovese, *A G-CSF functionalized PLLA scaffold for wound repair: An in vitro preliminary study*, Conf. Proc. IEEE Eng. Med. Biol. Soc., **2010** (2010), 843–846.

[76] M. S. Steinberg, *Reconstruction of tissues by dissociated cells. Some morphogenetic tissue movements and the sorting out of embryonic cells may have a common explanation*, Science, **141** (1963), 401–408.

[77] M. S. Steinberg, *Does differential adhesion govern self-assembly processes in histogenesis? Equilibrium configurations and the emergence of a hierarchy among populations of embryonic cells*, J. Exp. Zool., **171** (1970), 395–433.

[78] D. G. Stupack, *The biology of integrins*, Oncology, **21** (2007), 6-12.

[79] T. A. Ulrich, E. M. De Juan Pardo and S. Kumar, *The mechanical rigidity of the extracellular matrix regulates the structure, motility, and proliferation of glioma cells*, Cancer Res., **69** (2009), 4167–4174.

[80] M. C. Wake, C. W. Patrick and A. G. Mikos, *Pore morphology effects on the fibrovascular tissue growth in porous polymer substrates*, Cell. Transplant., **3** (1994), 339-343.

[81] K. Wolf, Y. I. Wu, Y. Liu, J. Geiger and E. Tam, *Multi-step pericellular proteolysis controls the transition from individual to collective cancer cell invasion*, Nat. Cell. Biol., **9** (2007), 893-904.

[82] K. Wolf, S. Alexander, V. Schacht, L. M. Coussens, U. H. Von Andrian, J. Van Rheenen, E. Deryugina and P. Friedl, *Collagen-based cell migration models in vitro and in vivo*, Semin. Cell. Dev. Biol., **20** (2009), 931–941.

[83] K. Wolf and P. Friedl, *Extracellular matrix determinants of proteolytic and non-proteolytic cell migration*, Trends Cell. Biol., **21** (2011), 736–744.

[84] K. Wolf, I. Mazo, H. Leung, K. Engelke, U. H. Von Andrian, E. I. Deryugina, A. Y. Strongin, E. B. Bröcker and P. Friedl, *Compensation mechanism in tumor cell migration mesenchymalamoeboid transition after blocking of pericellular proteolysis*, J. Cell. Biol., **160** (2003), 267–277.

[85] Y. L. Yang and L. J. Kaufman, *Rheology and confocal reflectance microscopy as probes of mechanical properties and structure during collagen and collagen/hyaluronan self-assembly*, Biophys. J., 96 (2009), 1566-1585.

[86] I. V. Yannas, E. Lee, D. P. Orgill, E. M. Skrabut, G. F. Murphy, *Synthesis and characterization of a model extracellular matrix that induces partial regeneration of adult mammalian skin*, Proc. Natl. Acad. Sci. U. S. A., 86 (1989), 933-937.

[87] M. H. Zaman, P. Matsudaira and D. A. Lauffenburger, *Understanding effects of matrix protease and matrix organization on directional persistence and translational speed in three-dimensional cell migration*, Ann. Biomed. Eng., **35** (2007), 91-100.

[88] M. H. Zaman, L. M. Trapani, A. L. Sieminski, D. Mackellar, H. Gong, R. D. Kamm, A. Wells, D. A. Lauffenburger and P. Matsudaira, *Migration of tumor cells in 3D matrices is governed by matrix stiffness along with cell-matrix adhesion and proteolysis*, Proc. Natl. Acad. Sci. U. S. A., **103** (2006), 10889–10894.

Received September 10, 2006; Accepted February 10, 2007.

E-mail address: marcosci1@alice.it
E-mail address: kata.wolf@gmx.de